ePublishing

ΕΘΝΙΚΟ ΚΕΝΤΡΟ ΤΕΚΜΗΡΙΩΣΗΣ
EKT NATIONAL DOCUMENTATION CENTRE

HNPS Advances in Nuclear Physics

Vol 9 (1998)

HNPS1998

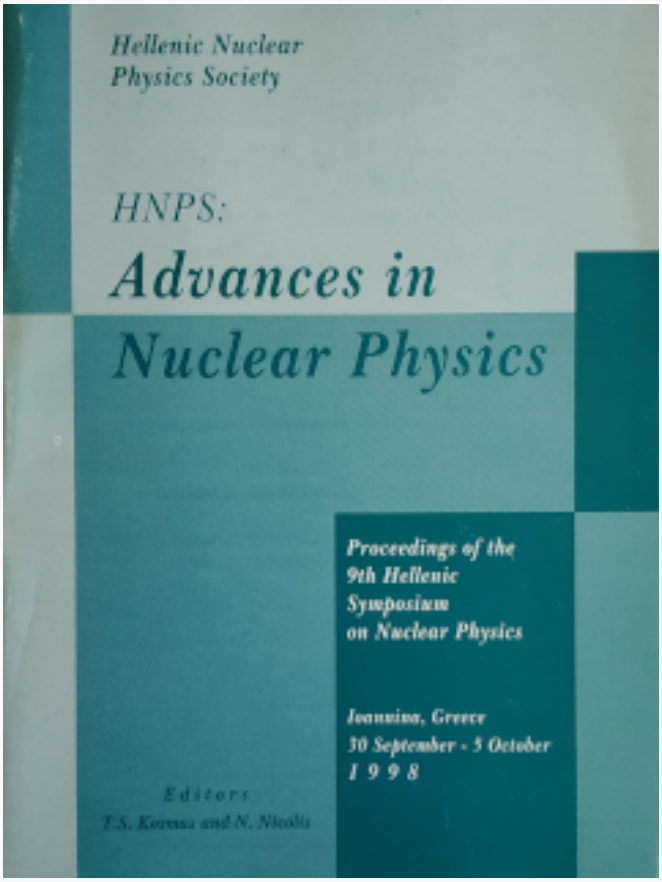

Applications of the relativistic mean-field model to finite nuclei.

G. A. Lalazissis

doi: 10.12681/hnps.2786

To cite this article:

Lalazissis, G. A. (2020). Applications of the relativistic mean-field model to finite nuclei. *HNPS Advances in Nuclear Physics*, *9*, 256–265. https://doi.org/10.12681/hnps.2786

https://epublishing.ekt.gr | **e-Publisher:** EKT | **Downloaded at:** 14/05/2026 19:46:10

Applications of the relativistic mean-field model to finite nuclei.

G.A. Lalazissis

Physik-Department der Technischen Universität München, D-85748 Germany

Abstract

The relativistic mean-field theory (RMF) provides a framework in which the nuclear many-body problem is described as a self-consistent system of nucleons and mesons. We review recent applications of the RMF theory to the structure of finite nuclei.

1 Introduction

RMF models have been successfully applied in calculations of nuclear matter and properties of finite nuclei throughout the periodic table. With only a few phenomenological parameters such theories are able to give a quantitative description of ground state properties of spherical and deformed nuclei at and away from the stability line. One of the advantage of the RMF theory is that the strength and the shape of the spin-orbit term are determined in a fully self-consistent way. Because the proper size of the spin-orbit splitting plays a crucial role in understanding the basic properties of nuclei, it follows that a proper treatment of the relativistic dynamics is warranted as is done in the RMF theory. Another example of the importance of relativistic dynamics is the fact that the near equuality (but opposite sign) of V and S leads to approximate pseudo-spin symmetry in nuclear spectra. The Relativistic Hartree Bogoliubov (RHB) model provides the frame for a unified and self-consistent description of mean-field and pairing correlations, which is necessary for a proper description of systems with extreme isospin values. Detailed calculations have been performed for a variety of nuclear structure phenomena [1]. Here we report some recent applications of the RMF model. In Section 2 the RMF formalism is given. In Sec. 3 the broken pseudo-spin symmetry is investigated. In Sec. 4 a brief description of the RHB model is provided. In Sec. 5 the formation of halos in light neutron rich nuclei is discussed, while in Sec. 6 the presence of a Λ hyperon in light drip line nuclei is examined.

2 The RMF formalism

In relativistic quantum hadrodynamics [2], a nucleus is described as system of Dirac nucleons that interact via exchange of virtual mesons and photons. The

Lagrangian density of the model is

$$\begin{aligned}\mathcal{L} &= \bar{\psi}\left(i\gamma\cdot\partial - m\right)\psi + \frac{1}{2}(\partial\sigma)^2 - U(\sigma) \\ &- \frac{1}{4}\Omega_{\mu\nu}\Omega^{\mu\nu} + \frac{1}{2}m_\omega^2\omega^2 - \frac{1}{4}\vec{\mathrm{R}}_{\mu\nu}\vec{\mathrm{R}}^{\mu\nu} + \frac{1}{2}m_\rho^2\vec{\rho}^2 - \frac{1}{4}\mathrm{F}_{\mu\nu}\mathrm{F}^{\mu\nu} \\ &- g_\sigma\bar{\psi}\sigma\psi - g_\omega\bar{\psi}\gamma\cdot\omega\psi - g_\rho\bar{\psi}\gamma\cdot\vec{\rho}\vec{\tau}\psi - e\bar{\psi}\gamma\cdot A\frac{(1-\tau_3)}{2}\psi\,. \end{aligned} \tag{1}$$

The Dirac spinor ψ denotes the nucleon with mass m. m_σ, m_ω, and m_ρ are the masses of the σ-meson, the ω-meson, and the ρ-meson, and g_σ, g_ω, and g_ρ are the corresponding coupling constants for the mesons to the nucleon. $U(\sigma)$ denotes the nonlinear σ self-interaction, and $\Omega^{\mu\nu}$, $\vec{R}^{\mu\nu}$, and $F^{\mu\nu}$ are field tensors [1,2]. The coupled equations of motion are derived from the Lagrangian density (1). The Dirac equation for the nucleons:

$$\begin{aligned} i\partial_t\psi_i &= \left[\boldsymbol{\alpha}\left(-i\boldsymbol{\nabla} - g_\omega\boldsymbol{\omega} - g_\rho\vec{\tau}\vec{\boldsymbol{\rho}} - e\frac{(1-\tau_3)}{2}\boldsymbol{A}\right) + \beta(m + g_\sigma\sigma)\right. \\ &\left. + g_\omega\omega_0 + g_\rho\vec{\tau}\vec{\rho}_0 + e\frac{(1-\tau_3)}{2}A_0\right]\psi_i \end{aligned} \tag{2}$$

and the Klein-Gordon equations for the mesons:

$$\left(\partial_t^2 - \Delta + m_\sigma^2\right)\sigma = -g_\sigma\rho_s - g_2\sigma^2 - g_3\sigma^3 \tag{3}$$

$$\left(\partial_t^2 - \Delta + m_\omega^2\right)\omega_\mu = g_\omega j_\mu \tag{4}$$

$$\left(\partial_t^2 - \Delta + m_\rho^2\right)\vec{\rho}_\mu = g_\rho\vec{j}_\mu \tag{5}$$

$$\left(\partial_t^2 - \Delta\right)A_\mu = ej_\mu^{\mathrm{em}}. \tag{6}$$

In the relativistic mean-field approximation, the nucleons described by single-particle spinors ψ_i $(i = 1, 2, ..., A)$ are assumed to form the A-particle Slater determinant $|\Phi\rangle$, and to move independently in the classical meson fields. The sources of the fields, i.e. densities and currents, are calculated in the *no-sea* approximation, the scalar density: $\rho_{\mathrm{s}} = \sum_{i=1}^{A}\bar{\psi}_i\psi_i$, the isoscalar baryon current: $j^\mu = \sum_{i=1}^{A}\bar{\psi}_i\gamma^\mu\psi_i$, the isovector baryon current: $\vec{j}^{\,\mu} = \sum_{i=1}^{A}\bar{\psi}_i\gamma^\mu\vec{\tau}\psi_i$, the electromagnetic current for the photon-field: $j_{\mathrm{em}}^\mu = \sum_{i=1}^{A}\bar{\psi}_i\gamma^\mu\frac{1-\tau_3}{2}\psi_i$. The summation is over all occupied states in the Slater determinant $|\Phi\rangle$. Negative-energy states do not contribute to the densities in the *no-sea* approximation of the stationary solutions. It is assumed that nucleon single-particle states do not mix isospin.

The ground state of a nucleus is described by the stationary self-consistent solution of the coupled system of equations (2)–(6), for a given number of nucleons and a set of coupling constants and masses. In this paper, we report results obtained with the parameter set NL3 of the mean field Lagrangian. The NL3 force has been derived recently [3] by fitting ground state properties of a large number of spherical nuclei. Properties calculated with the NL3 effective interaction are found to be in very good agreement with experimental data for nuclei at and away from the line of β-stability [4,5].

3. Pseudo-spin symmetry in RMF theory

Pseudospin symmetry has been discovered in nuclear physics 30 years ago [6–8]. Recently, Ginocchio [9] suggested that the pseudo-spin symmetry may arise due to near equality in magnitude of attractive scalar and repulsive vector fields in relativistic mean theory. This has revived the activity related to the understanding of the origin of this symmetry in real nuclei. The concept of pseudo-spin symmetry [6,7] is based on the experimental observation of the existence of quasi-degenerate doublets of normal parity orbitals $(n,\ \ell,\ j=\ell+\frac{1}{2})$ and $(n-1,\ \ell+2,\ j=\ell+\frac{3}{2})$ such as $(4s_{1/2},\ 3d_{3/2})$, $(3d_{5/2},\ 2g_{7/2})$ etc., in the same major shell. Since for spherical systems the quantum numbers j^{π} are conserved, the pseudo-spin angular momenta $(\tilde{\ell},\ \tilde{s}=1/2)$ satisfy $\tilde{j}=j=\tilde{l}\pm\frac{1}{2}$.

It is straightforward to write the coupled baryon spinor and the mesons mean field equations. Starting from the Dirac equation for the single nucleon radial wave function with the spherical attractive scalar $(S=-g_{\sigma}\sigma)$ and the repulsive vector $(V=g_{\omega}\omega)$ potentials and following the standard procedure, by eliminating the small components (g_i), the large components (f_i) obey the following second order differential equation:

$$\begin{aligned}&\left\{-\nabla^2-\frac{S'+V'}{2m-E-(S+V)}\left(\frac{\partial}{\partial r}+\frac{\kappa_i+1}{r}\right)\right\}f_i\\ =\ &-(2m-E-(S+V))\,(E-(S-V))\,f_i.\end{aligned}\tag{7}$$

Here the eigenvalues denoted by κ_i, of the operator $-\beta(\mathbf{\Sigma}\cdot\mathbf{L}+1)$ are given by

$$\kappa_i\ =\ \mp\left(j_i+\frac{1}{2}\right)\qquad\text{for}\qquad j_i=\ell_i\pm\frac{1}{2}\ ,\tag{8}$$

and S' (V') are the derivatives of the potentials S $(V\ )$ with respect to r. The binding energy $E\geq 0$ is measured with respect to the nucleon mass M in natural units $\hbar=c=1$. On the other hand eliminating the large component f_i we have for the small component g_i the following second order differential equation:

$$\begin{aligned}&\left\{-\nabla^2-\frac{S'-V'}{E-(S-V)}\left(\frac{\partial}{\partial r}-\frac{\kappa_i-1}{r}\right)\right\}g_i\\ =\ &(2m-E-(S+V))\,(E-(S-V))\,g_i.\end{aligned}\tag{9}$$

For the case of equal strengths, $S=V$, the Eq. (9) reduces to:

$$-\nabla^2 g_i+E(S+V)\,g_i=E(2m-E)\,g_i.\tag{10}$$

Clearly Eq. (10) has an energy dependent potential $(E(V+S))$ and has the eigenvalue $E(2m-E)$. After scaling the radial variable $r=x/(\sqrt{E})$, the potential has a complicated $(\sqrt{E})$ dependence *i.e.*, $S\left(x/\sqrt{E}\right)+V\left(x/\sqrt{E}\right)$. In such a situation this equation (10) is no longer a normal Schrödinger eigenvalue equation. Further, it is obvious that in this equation all solutions with "bound" states in the Fermi sea with $E\geq 0$ are shifted to one degenerate eigenvalue with $E=0$, which, in fact, is not bound. The corresponding wave functions are not normalizable. This indeed is an unphysical situation. This equation is the same as the equation (3) of Ref. [9] in the scaled variable x when written in terms of the partial waves and using the relation $\ell(\ell+1)=\kappa(\kappa-1)$. Here ℓ, the angular momentum of

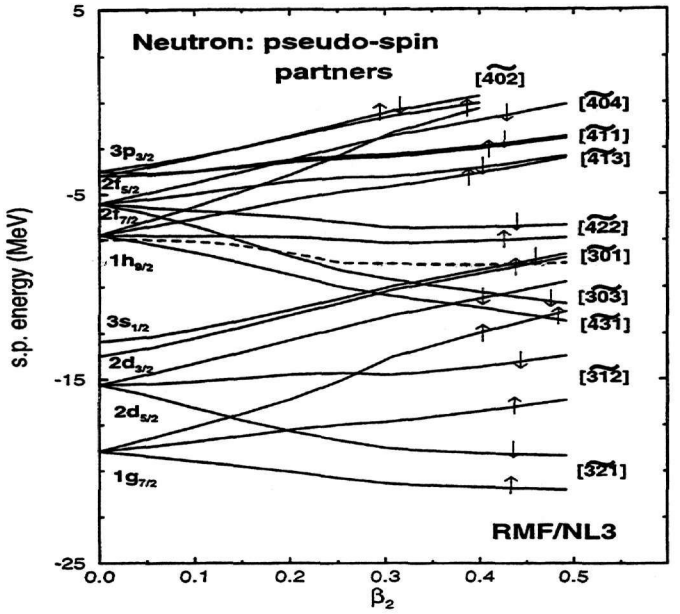

Figure 1. Single particle energies of the deformed Dirac equation for the neutrons in the nucleus ^{154}Dy as a function of the quadrupole deformation parameter β_2. Asymptotic pseudo-spin quantum numbers are given and the pseudo-spin partners are indicated by arrows $\uparrow$ and $\downarrow$

the lower component g_i is identified with the pseudo-spin angular momentum ($\tilde{\ell}$). This is the pseudo-spin symmetry limit of Ref. [9], where the doublets $j = \tilde{\ell} \pm 1/2$ with the same $\tilde{\ell}$ are degenerate. However, in this limit only the Dirac sea states exist and no Dirac valence bound states and therefore contradicts reality. According to these considerations in all realistic situations the pseudo-spin symmetry must be broken. Therefore the question arises, to which extent it is broken in real nuclei. So far only the spherical case has been investigated for square well potentials [9] and for spherical solutions of the RMF equations[10].

In the present work we investigate the broken pseudo-spin symmetry in deformed nuclei within the relativistic mean field approach. For our study, ^{154}Dy as a representative of deformed nuclei. We use in our calculations the Lagrangian parameter set NL3[3] which successfully reproduces the ground state properties of nuclei, spread over the entire periodic table. Constrained relativistic Hartree calculations have been carried out for the nucleus ^{154}Dy. Numerical details are given in Refs. [11] and [12]. Pairing correlations are treated in the constant gap approximation.

The energies of the bound neutron pairs of orbitals corresponding to pseudo-spin doublets are plotted against the deformation β_2 ranging from 0.0 to 0.5 in Fig.1. The asymptotic Nilsson quantum numbers $[N, n_3, \Lambda, \Omega]$ are good for large values of the deformation β_2. The pseudo-spin doublets $[\tilde{N}, \tilde{n}_3, \tilde{\Lambda}, \tilde{\Omega} = \tilde{\Lambda} \pm 1/2]$ [13] are indicated by $[\tilde{N}, \tilde{n}_3, \tilde{\Lambda}]$ $\uparrow$ and $\downarrow$ in the figure. For zero deformation ($\beta_2 = 0$) the orbitals are indicated by the

corresponding spherical states. The figure reveals the following:
a) The energy splitting between the pseudo-spin partners is smaller for the valence orbitals and for the partners just below the Fermi surface.
b) This energy difference is relatively larger for the partners having larger pseudo-spin angular momentum ($\tilde{\ell}$).
c) In general, this separation stays almost constant and does not vary with deformation after reasonable value of β_2.
d) The energy difference between the $\downarrow$ and the $\uparrow$ partners always remains positive except for [$\tilde{4}0\tilde{4}$], where there is crossing at around $\beta = 0.3$. Such a crossing is not very unusual, it has also been observed in Ref.[13].

These systematics are consistent with those observed in the spherical nuclei. A similar plot for the proton pseudo-spin doublets reveals identical systematics as those observed for the neutron case [14]. It is noted that similar calculations have also been carried out for other deformed nuclei and they show identical systematics. In conclusion, it is shown in the relativistic mean field framework that quasi-degenerate pseudo-spin doublets do exist near the fermi surface for both spherical and deformed nuclei. The pseudo-spin symmetry is restored better and better as one moves closer to the continuum limit. These conclusions confirm the findings of Ginocchio [9,15].

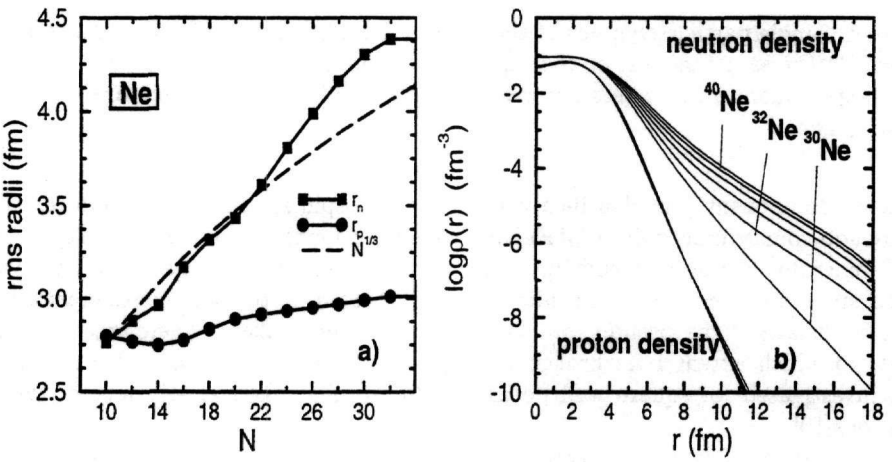

Figure 2. Calculated *rms* radii (a) and proton and neutron density distribution (b) for Ne isotopes.

4. The Relativistic Hartree-Bogoliubov model

The relativistic extension of the HFB theory is described in ref.[16] Independent quasi-particles are introduced and the ground state of a nucleus $|\Phi>$ is represented as the vacuum with respect to these quasi-particles. The quasi-particle operators are defined by a unitary Bogoliubov transformation of the single-nucleon creation and annihilation op-

erators. The generalized single-particle hamiltonian of HFB theory contains two average potentials: the self-consistent field $\hat{\Gamma}$ which encloses all the long range *ph* correlations, and a pairing field $\hat{\Delta}$ which sums up the *pp*-correlations. In the Hartree approximation for the self-consistent mean field, the Relativistic Hartree-Bogoliubov (RHB) equations read

$$\begin{pmatrix} \hat{h}_D - m - \lambda & \hat{\Delta} \\ -\hat{\Delta}^* & -\hat{h}_D + m + \lambda \end{pmatrix} \begin{pmatrix} U_k \\ V_k \end{pmatrix} = E_k \begin{pmatrix} U_k \\ V_k \end{pmatrix}. \tag{11}$$

where $\hat{h}_D$ is the single-nucleon Dirac hamiltonian, and m is the nucleon mass. U_k and V_k are quasi-particle Dirac spinors, and E_k denote the quasi-particle energies. The RHB equations are non-linear integro-differential equations. They have to be solved self-consistently, with potentials determined in the mean-field approximation from solutions of Klein-Gordon equations for mesons and Coulomb field:

$$\begin{aligned} [-\Delta + m_\sigma^2]\,\sigma(\mathbf{r}) &= -g_\sigma \sum_{E_k>0} V_k^\dagger(\mathbf{r})\gamma^0 V_k(\mathbf{r}) \\ &\quad -g_2\,\sigma^2(\mathbf{r}) - g_3\,\sigma^3(\mathbf{r}), \qquad (12) \\ [-\Delta + m_\omega^2]\,\omega^0(\mathbf{r}) &= -g_\omega \sum_{E_k>0} V_k^\dagger(\mathbf{r}) V_k(\mathbf{r}), \qquad (13) \\ [-\Delta + m_\rho^2]\,\rho^0(\mathbf{r}) &= -g_\rho \sum_{E_k>0} V_k^\dagger(\mathbf{r})\tau_3 V_k(\mathbf{r}), \qquad (14) \\ -\Delta\, A^0(\mathbf{r}) &= e \sum_{E_k>0} V_k^\dagger(\mathbf{r}) \frac{1-\tau_3}{2} V_k(\mathbf{r}). \qquad (15) \end{aligned}$$

The source terms are sums of bilinear products of baryon amplitudes. The sums run over all positive energy states. The system of equations is solved self-consistently in coordinate space by discretization on the finite element mesh [17]. The pairing field $\hat{\Delta}$ in (1) is defined

$$\Delta_{ab}(\mathbf{r},\mathbf{r}') = \frac{1}{2}\sum_{c,d} V_{abcd}(\mathbf{r},\mathbf{r}')\kappa_{cd}(\mathbf{r},\mathbf{r}'). \tag{16}$$

where $V_{abcd}(\mathbf{r},\mathbf{r}')$ are matrix elements of a general two-body pairing interaction and $\kappa_{cd}(\mathbf{r},\mathbf{r}')$, is the pairing tensor, defined as

$$\kappa_{cd}(\mathbf{r},\mathbf{r}') := \sum_{E_k>0} U_{ck}^*(\mathbf{r}) V_{dk}(\mathbf{r}'). \tag{17}$$

The eigensolutions of (1) form a set of orthogonal and normalized single quasi-particle states. The corresponding eigenvalues are the single quasi-particle energies. The self-consistent iteration procedure is performed in the basis of the quasi-particle states. The resulting quasi-particle eigenspectrum is then transformed into the canonical basis of the single-particle states, in which the RHB ground-state takes the separable BCS form. The transformation determines the energies and occupation probabilities of the canonical states. In this work, in the particle-particle (*pp*) channel the pairing interaction is approximated by a two-body finite range interaction of Gogny type [18].

$$\begin{aligned} V^{pp}(1,2) &= \sum_{1,2} e^{-(\mathbf{r}_1-\mathbf{r}_2/\mu_i)^2}\,(W_i + B_i P^\sigma \\ &\quad -H_i P^\tau - M_i P^\sigma P^\tau), \qquad (18) \end{aligned}$$

with the set D1S [18] for the parameters μ_i, W_i, B_i, H_i and M_i $(I = 1,2)$.

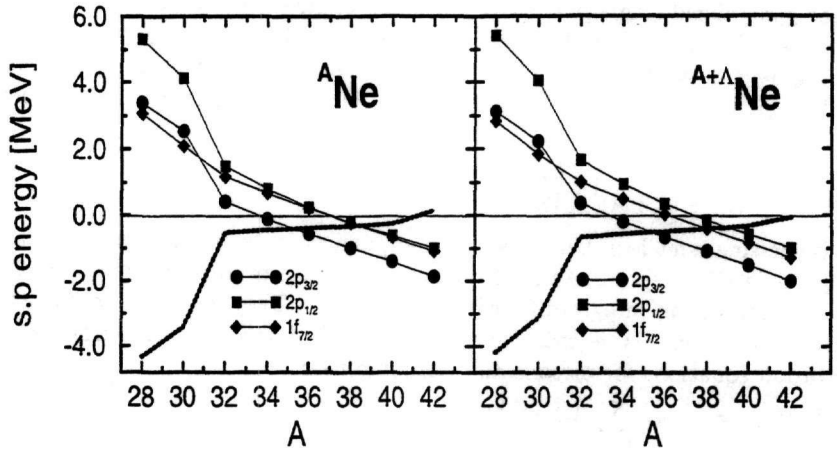

Figure 3. 1f-2p single-particle neutron levels in the canonical basis for the Ne (a), and $Ne + \Lambda$ (b) isotopes.

Neutron halo in light nuclei

In some loosely bound systems at the drip-lines, the neutron density distribution displays an extremely long tail: the neutron halo. The resulting large interaction cross sections have provided the first experimental evidence for halo nuclei [19]. The neutron halo phenomenon has been studied with a variety of theoretical models [20,21]. For very light nuclei in particular, models based on the separation into core plus valence space nucleons (three-body Borromean systems) have been employed. In heavier neutron-rich nuclei one expects that mean-field models should provide a better description of ground-state properties. In a mean-field description, the neutron halo and the stability against nucleon emission can only be explained with the inclusion of pairing correlations. Both the properties of single-particle states near the neutron Fermi level, and the pairing interaction, are important in the formation of the neutron halo. The details of the formation of the neutron halo in Ne isotopes have been studied in Ref. [22,23]. In Fig. 2a the rms radii for Ne isotopes are plotted as functions of neutron number. Neutron and proton rms radii are shown, and the $N^{1/3}$ curve normalized so that it coincides with the neutron radius in ^{20}Ne. The neutron radii follow the mean-field $N^{1/3}$ curve up to $N \approx 22$. For larger values of N the neutron radii display a sharp increase, while the proton radii stay practically constant. This sudden increase in neutron rms radii has been interpreted as evidence for the formation of a multi-particle halo. The phenomenon is also observed in the plot of proton and neutron density distributions (Fig. 2b). The proton density profiles do not change with the number of neutrons, while the neutron density distributions display an abrupt change between ^{30}Ne and ^{32}Ne. The microscopic origin of the neutron halo has been found in a delicate balance of the self-consistent mean-field and the pairing field. This is shown in Fig. 3a, where the neutron single-particle states $1f_{7/2}$, $2p_{3/2}$ and

$2p_{1/2}$ in the canonical basis, and the Fermi energy are plotted as function of the neutron number. For $N \leq 22$ the triplet of states is high in the continuum, and the Fermi level uniformly increases toward zero. The triplet approaches zero energy, and a gap is formed between these states and all other states in the continuum. The shell structure dramatically changes at $N \geq 22$. Between $N = 22$ and $N = 32$ the Fermi level is practically constant and very close to the continuum. The addition of neutrons in this region of the drip does not increase the binding. Only the spatial extension of neutron distribution displays an increase. The formation of the neutron halo is related to the quasi-degeneracy of the triplet of states $1f_{7/2}$, $2p_{3/2}$ and $2p_{1/2}$. The pairing interaction promotes neutrons from the $1f_{7/2}$ orbital to the 2p levels. Since these levels are so close in energy, the total binding energy does not change significantly. Due to their small centrifugal barrier, the $2p_{3/2}$ and $2p_{1/2}$ orbitals form the halo.

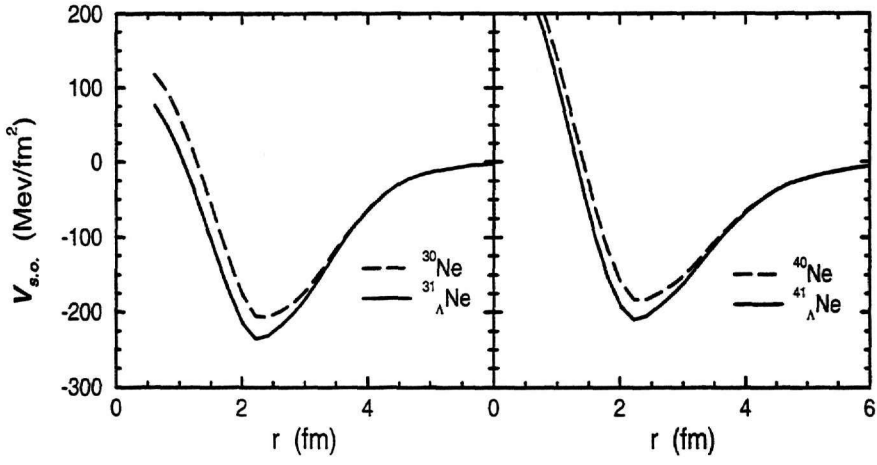

Figure 4. Radial dependence of the spin-orbit potential in self-consistent solutions for the ground-states of Ne, and $Ne + \Lambda$ isotopes.

5. Light Λ hypernuclei near the neutron drip

The effects of the Λ hyperon on Ne isotopes with neutron halo has also been studied [24]. The Dirac equation for the Λ particle has the following form:

$$[-i\alpha\nabla + \beta(m_\Lambda + g_{\sigma\Lambda}\sigma(\mathbf{r})) + g_{\omega\Lambda}\omega^0(\mathbf{r})]\psi_\Lambda = \epsilon_\Lambda\psi_\Lambda \tag{19}$$

The coupling constants for the Λ particle are from Ref. [25], where the relativistic mean-field theory was used to study characteristics of Λ, Σ and Ξ hypernuclei. While the values for the $g_{\omega Y}$ coupling constants were determined from the naive quark model, that is $g_{\omega\Lambda} = \frac{2}{3}g_{\omega N}$; the values of $g_{\sigma Y}$ were deduced from the available experimental information of hyperon binding in the nuclear medium. For the Λ hyperon $g_{\sigma\Lambda}$ was fitted to reproduce the binding energy of a Λ in the $1s$ state of $^{17}_{\Lambda}$O: $g_{\sigma\Lambda} = 0.621 g_{\sigma N}$. The coupling constant

determined from only this experimental quantity gives a reasonable description of binding energies in Λ hypernuclei for a wide range of mass number.

In Fig. 3b we illustrate the effect of the Λ hyperon on the triplet of neutron states that form the halo: $1f_{7/2}$, $2p_{3/2}$ and $2p_{1/2}$, and on the Fermi level. The energies are displayed as function of the core mass number A_c. Due to the extra binding provided by the Λ, the single-neutron energies and the Fermi level are lower. The most important effect that we observe, however, is that the Fermi level is negative for the isotope $^{42+\Lambda}$Ne. Without the Λ, the nucleus ^{42}Ne was unbound.

Although the inclusion of the Λ does not produce excessive changes in bulk properties of these nuclei, it can shift the neutron drip by stabilizing an otherwise unbound core nucleus at the drip-line. The microscopic mechanism through which additional neutrons are bound to the core originates from the increase in magnitude of the spin-orbit term in presence of the Λ particle. The Λ in its ground state produces only a fractional change in the central mean-field potential. On the other hand, through a purely relativistic effect, it notably changes the spin-orbit term in the surface region, providing additional binding for the outermost neutrons. This is shown in Fig. 4 where the radial dependence of the spin-orbit potential for the ground states of ^{30}Ne, ^{40}Ne and $^{31+\Lambda}$Ne, $^{41+\Lambda}$Ne isotopes is displayed. It is seen that for the corresponding Λ-hypernuclei (solid lines) the spin-orbit term displays an increase in magnitude of about 10% (smaller as we approach the drip line ($^{41+\Lambda}$Ne)). The effect can be illustrated on the example of ^{30}Ne and the corresponding hypernucleus $^{31}_{\Lambda}$Ne. The mean field potential, in which the nucleons move, results from the cancelation of two large meson potentials: the attractive scalar potential S and the repulsive vector potential V: V+S. The spin-orbit potential, on the other hand, arises from the very strong anti-nucleon potential V-S. Therefore, while in the presence of the Λ the changes in V and S cancel out in the mean-field potential, they are amplified in V_{ls}. For the core ^{30}Ne the values of the scalar (S) and vector (V) potential in the center of the nucleus are -380 MeV and 308 MeV, respectively. For $^{31}_{\Lambda}$Ne the corresponding values are: -412 MeV and 336 MeV. The addition of the Λ particle changes the value of the mean-field potential in the center of the nucleus by 4 MeV, but it changes the anti-nucleon potential by 60 MeV. This is reflected in the corresponding spin-orbit term of the effective potential, which provides more binding for states close to the Fermi surface. The additional binding stabilizes the hypernuclear core.

REFERENCES

1. P. Ring, Progr. Part. Nucl. Phys. **37** 193 (1996).
2. B.D. Serot and J.D. Walecka, Int. J. Mod. Phys. **E6** 515(1997).
3. G. A. Lalazissis, J. König and P. Ring, Phys. Rev. C **55** 540 (1997) .
4. G.A. Lalazissis, D. Vretenar, and P. Ring, Phys. Rev. C **57**, 2294 (1998).
5. G.A. Lalazissis, S. Raman and P. Ring, At. Data Nucl. Data Tables **71** 1 (1999).
6. K.T. Hecht, A. Adler; Nucl. Phys. **A137**, 129 (1969).
7. A. Arima, M. Harvey, K. Shimizu; Phys. Lett. **B30**, 517 (1969).
8. R.D. Ratna Raju, J.P. Draayer, K.T. Hecht; Nucl. Phys. **A202**, 433 (1973).
9. J. N. Ginocchio, Phys. Rev. Lett. **78**, 436 (1997).
10. J. N. Ginocchio and D. G. Madland, Phys. Rev. C **57**, 1167 (1998)

11. Y. K. Gambhir, P. Ring and A. Thimet, Ann. Phys. (N.Y.) **198,** 132 (1990).
12. P. Ring, Y.K. Gambhir, and G.A. Lalazissis Comp. Phys. Comm. **105**, 77 (1997).
13. A. Bohr, I. Hamamoto and B. R. Mottelson, Phys. Scr. **26,** 267 (1982).
14. G.A. Lalazissis, Y. Gambhir, J. Maharana, Y. Warke, P. Ring Phys. Rev. C **58** R45 (1998).
15. J. N. Ginocchio and A. Leviatan, Phys. Lett. **B 425** 1 (1998)
16. H. Kucharek and P. Ring; Z. Phys. **A 339** 23 (1991).
17. W. Pöschl, D. Vretenar and P. Ring Comput. Phys. Commun. **103** 217 (1997).
18. J. F. Berger, M. Girod and D. Gogny Nucl. Phys. **A428** 32 (1984).
19. I. Tanihata et al., *Phys. Rev. Lett.* **55**, 2676 (1985); *Phys. Lett.* **B206**, 592 (1988).
20. I. Tanihata, *Prog. Part. Nucl. Phys.* **35**, 505 (1995).
21. P. Hansen, A.S. Jensen, and B. Jonson, *Annu. Rev. Nucl. Part. Phys.* **45**, 591 (1995).
22. W. Pöschl, D. Vretenar, G.A. Lalazissis, and P. Ring, *Phys. Rev. Lett.* **79**, 3841 (1997).
23. G.A. Lalazissis, D. Vretenar, W. Pöschl, and P. Ring, *Nucl. Phys.* **A632**, 363 (1998).
24. D. Vretenar, W. Pöschl, G.A. Lalazissis, and P. Ring, Phys. Rev. C **57**, R1060 (1998).
25. J. Mareš and B. K. Jennings; Phys. Rev. C **49**, 2472 (1994).